An Investigation of a Morphing Flapped Wing

1st EDITION OF THE AEROSPACE EUROPE CONFERENCE – AEC2020

BORDEAUX, FRANCE / 25 -28 FEBRUARY

Fakhreddine Madi(1), Zac Kanaa(2), Pritesh Narayan(3), Yufeng Yao(4)

(1) *MEng Student at University of the West of England*, UWE Bristol, Coldharbour Lane, Bristol BS16 1QY, United Kingdom, Email: Fakhreddinemadi@outlook.com

(2) *Aerospace and Thermofluids Technician,* UWE Bristol, Coldharbour Lane, Bristol BS16 1QY, United Kingdom Email: Zac.kanaa@uwe.ac.uk

(3) *Associate Head of Department - Aerospace, Aviation and Management Cluster Leader* UWE Bristol, Coldharbour Lane, Bristol BS16 1QY, United Kingdom, Email: Pritesh.Narayan@uwe.ac.uk

(4) *Professor in Aerospace Engineering*, UWE Bristol, Coldharbour Lane, Bristol BS16 1QY, United Kingdom, Email: Yufeng.Yao@uwe.ac.uk

Keywords: morphing wing, wind tunnel, improving wing efficiency

Abstract

This study investigated the design, development, and validation of an alternative method to achieve morphing in wings through the implementation of a sliding mechanism concept. Performance was tested at a specific Reynolds number (Re = 0.62 × 10^6). Manufacturing an initial wing that incorporated a modular flap design allowed both hinge and morphing flap to be tested using the same primary setup. A subsonic wind tunnel was used to experimentally test the two setups at the same conditions. The goal of this study was to verify the experimental findings against Computational Fluid Dynamics results completed by Abdessemed et al. regarding statically set flaps. Results of this study showed trends that matched [1] despite the slightly different set up used. This study confirmed that such designs could achieve greater performance at lower angles of attack.

1. Introduction

Modern aircraft have almost reached a point where conventional aerodynamic improvements are hitting a barrier [1]; however, aerospace industries are being pressured to develop more environmentally friendly aircraft due to global warming and climate change, and therefore must overcome this barrier in development.

One of the major influences that is pushing the industry to become more environmentally friendly is Flightpath 2050 [2]. The Flightpath 2050 initiative aims to protect the environment by improving aircraft efficiency set by the European Commission in 2011. Scientists and engineers have been trying to recreate aircraft designs using pioneering technologies such as lighter materials, unique fuselage arrangements and adaptive structures that can meet the requirements of different flight envelopes. Adaptive structures are one of the most recent fields that researchers are concentrating on. Advantages and challenges regarding adaptive structures will be discussed further to obtain a better understanding of this field.

Macaraeg, M. et al. investigated elastically shaped future air vehicles and identified several concepts with different features such as having a drooped-wing, inflected-wing, squashed-fuselage drooped wing and variable camber [3]. Each concept showed variable drag reduction improvements and the latter concept exhibited a drag reduction of over 50% with respect to conventional flap systems during aerodynamic simulations. Moreover, other studies by [3] [4] dictated that existing gaps at the end of the control surfaces in both span and chord wise direction created increased vortexes and contributed to substantial noise while the aircraft is in take-off and landing configurations.

The main advantages that one could expect from such morphing wings can include: increased operational flexibility within the mission

parameters; and additional aerodynamic efficiency from optimised lift-to-drag ratio resulting in increased cruising range. However, the additional complexities in the morphing design process which will need to be considered are: materials that could be adapted for the required morphing shape; optimization that will allow the best improvements from configuration; and precise measurements of aerodynamic forces to estimate whether or not the aerodynamic improvements exceed the added complexity of the morphing wing.

The aims of this project are to design, manufacture, and experimentally test a morphing camber wing (3D) to verify the aerodynamic effects of such a naturally occurring design in comparison to conventional designs across a range of controlled conditions. Deriving the objectives from the aims of this study were split into three main sections: design, manufacture, and testing. The objectives of this project could be summed up in the following points:

- Design: Adjusting the model to fit requirement for comparison.
- Manufacture: Building a model wing that can integrate a traditional single hinged flap and a morphing flap.
- Testing: Wind tunnel testing and Computational Fluid Dynamics (CFD) comparison analysis under different modes of flight.

The project was inspired by birds and their ability to actively morph their wing camber to adjust for natural changes in the airflow to maintain their necessary flight path. Companies such as 'FlexSys' have been researching potential wing designs that could replace conventional flaps and slats by using actively changing cambers via smart martials and intricate designs. Conducting experiments that could be verified by [1] may further support such projects, thus experimental validation of [1] is proposed in this study.

This paper is structured in the following manner: in section 2 the morphing wing design is briefly outlined whilst section 3 summarises the manufacturing process. Section 4 outlines the test setup before experimental and CFD results are presented in Section 5. In section 6 conclusions of this study are presented.

2. Morphing Wing Design

The project required a baseline NACA 0012 wing that has a removable trailing edge. This will allow a comparison between morphing aerofoil and its baseline. MATLAB simulation software was used to generate the deflection angle to match the required relative angle needed for comparison, measurements of relative angle in degrees to percent length relative to chord shown in Fig. 1. It is necessary to have a numerical presentation of angle deflection to enable the proper data to be captured need to allow an accurate Computer Aided Design (CAD) model designs and CFD simulation [14].

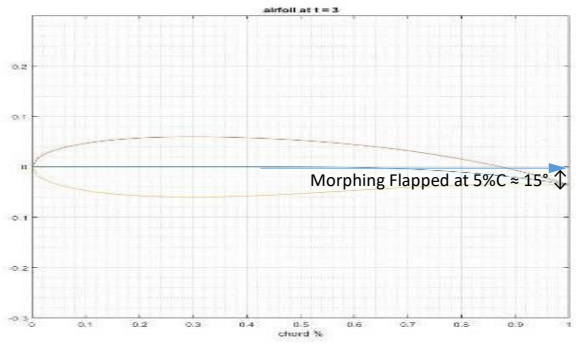

Figure 1. MATLAB Code Projection of NACA0012 with Morphing flap at 5% chord length equivalent to Flap at 15° Cambered at 75% chord length.

Manufacturing a wing with the trailing edge design attachment allowed removal of the flap to be tested in each case and helped obtain comparable results. The final configuration of this study was based on previous work done [5]. Figs. 2-3-4 show the design process from initial prototype concept to final CAD and manufactured design for a morphing wing. The final manufactured wing at maximum deflection as seen in Fig. (5).

Figure 2. Max Camber initial prototype

Figure 3. Zero Camber initial prototype

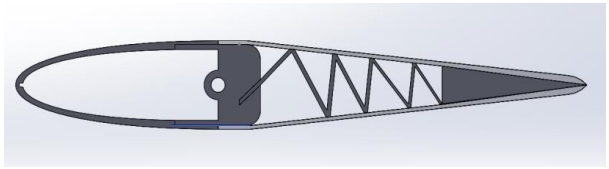

Figure 4. Final CAD Model on Solidworks Software

Figure 5. Final manufactured prototype at max camber

To be able to compare trends with [1], this study implements a similar configuration to [1]. Initially, use of the same chord length and span resulted in a design that was able to undergo wind tunnel testing. Scaling was taken into account since blockage effect could play a role. Leaving more than 60% of the wind tunnel clear [15] required a span of more than 420mm as well as chord length of 500mm. Fig. 6 is the initial scaled 3D model design that allows the switching of flap configuration and structurally support the loads in the wind tunnel by distributing the loads. Using the program JavaFoil, the coordinates of the aerofoil NACA0012 were scaled to the requirements and imported to SolidWorks.

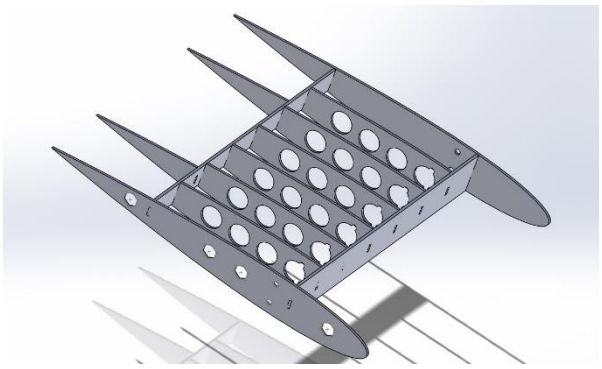

Figure 6. Final 3D internal section layout

Comparing this 3D model to the study by [1] shows similar design configuration. Figs. 7-8 where taken from [1] to allow visual and actual measurement comparison of models.

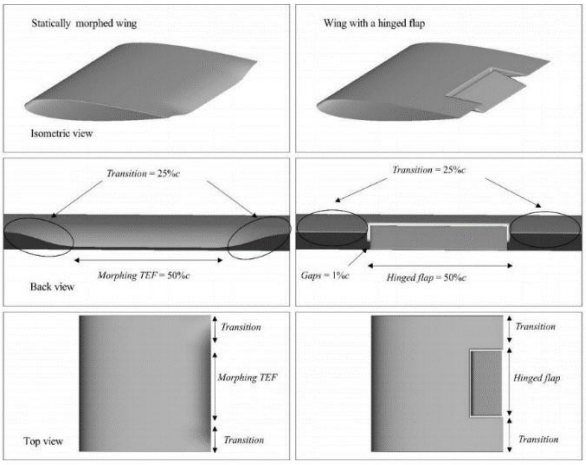

Figure 7. 3D CAD Models [1]

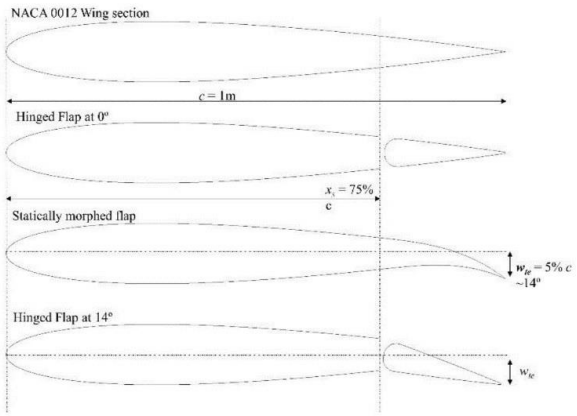

Figure 8. Chord projection of NACA morphing relative to hinged flap deflection [1]

3. Morphing Wing Manufacturing

Starting with the core skeletal structure being cut out of Medium-Density Fibreboard (MDF), the leading and part of the static trailing edge were filled by foam. Fig. 9 shows how the assembly of foam and MDF where combined together to create the final model for testing.

Figure 9. Internal and assembly of final prototype

Figure 10. Single hinged flap wing

Figure 11. Adjusted internal morphing flap wing

Figure 12. Final Morphing wing

The final single hinged flap configuration can be seen in Fig. 10 and Fig. 11 shows the internal structure for the final morphing flap wing; solar film was used to cover both configurations. The final 3D morphing flapped wing needed an additional flexible skin to cover the gapped area where the morphing component meets with the rest of the trail edge. Using latex for this area enabled the smooth continuous surface (Fig. 12). The wing was attached to the wind tunnel via a circular plate that can be seen in Fig. 13.

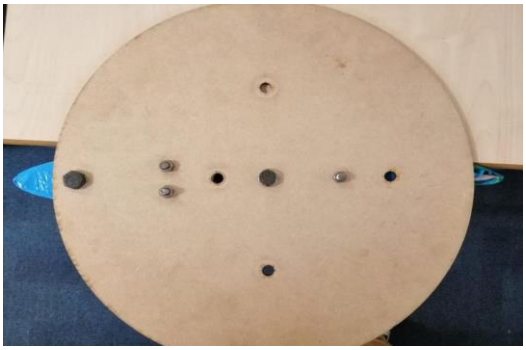

Figure 13. Circular plate attachment to symmetry plane.

4. Testing Setup

Aircraft moving in a fluid medium (air for this setup) disturbs the flow near the surface of the aircraft. Molecule particles that are closer to the surface have lower velocities than those further away from the surface. This effect creates a boundary layer where aerodynamic forces are produced between the surface and the medium, dependent on speed and density of the medium [14]. In addition, other parameters that need to be calculated first are the Reynolds numbers using Eq. 1 of flight from [14].

$$Re = \frac{\rho \times V \times L}{\mu} \quad [1]$$

Where ρ, is air density at sea level at 20 ^{o}C and assumed to have a value of 1.23 $\frac{kg}{m^3}$ [4]. V; is the velocity at which the tests were conducted. 18 $\frac{m}{s}$ was chosen for *V* as this value was used previously to match the Reynolds number. L; is the chord length of the wing and selected due to manufacturing and wind tunnel blockage constraints. μ; is the dynamic viscosity at 20 ^{o}C and at sea level atmospheric pressure will be assumed to have a value of 1.789 e-5 $\frac{kg}{ms}$

Using the above values an initial Reynolds number was calculated to be:

$$Re = \frac{\rho \times V \times L}{\mu} = 615{,}684$$

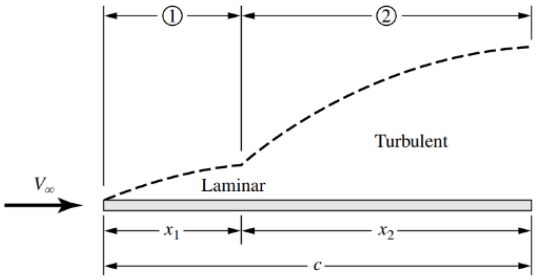

Figure 14. Boundary layer regions from [14]

Viscous flow is most significant near the wall surface. The phenomenon can be clearly seen in Fig. 14 where the boundary layer is split in to a laminar and turbulent region. To check where the transition, $X_{cr} = x_1$, is happening in this study the following Eq. 2 from [14] was used;

$$Re_{X_{cr}} = \frac{\rho_{inf} * V_{inf} * X_{cr}}{\mu_{inf}};\ X_{cr} = \frac{\mu_{inf} * Re_{X_{cr}}}{\rho_{inf} * V_{inf}} = 0.4974\ m \quad [2]$$

This indicates that given our reference values, the transition point should be located on 99.48% of the chord. This will allow a mostly laminar flow across the surface.

$$C_L = \frac{2\ Lift}{\rho \times V^2 \times A} = \frac{Lift}{q \times A} \quad [3]$$

$$C_D = \frac{2\ Drag}{\rho \times V^2 \times A} = \frac{Drag}{q \times A} \quad [4]$$

Lift on aerofoils is mainly due to the pressure distribution across the surface [14]. This typically occurs when a lift force is perpendicular to the path of flight, but the drag forces is in the opposing direction. Eq. (3-4) show the relation of the coefficients with their relative forces.

The total boundary layer thickness (δ) for incompressible flow can be calculated using the following equation from [14]

$$\delta = \frac{5.0\ x}{\sqrt{Re_x}} = 0.00318611\ m \quad [5]$$

Where *x* is constant factor (value of 5), and assuming $Re_{X_{cr}} = Re_x$ from the previous equation Eq. 2 [14]

The CFD section for this study was split into three main categories, domain, turbulance mode and mesh. The domain should resembled the working section of the wind tunnel as seen in Fig.15. Turbulance model that should be used was determined by the best simulation performance with acceptable accuracy in results. The mesh divided the domain into small sized geometrical fragments were the boundary layer near the surface of the aerofoil was sized to match

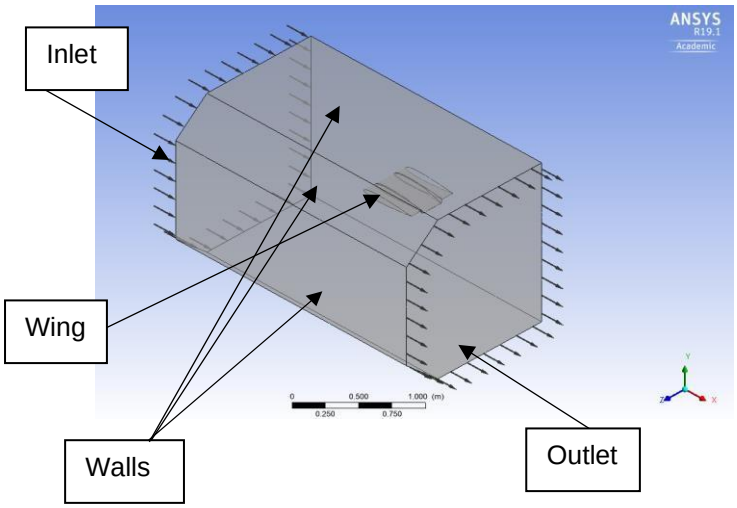

Figure 15. Domain of the working section in ANSYS

theoretical calculation completed in Eq. 5 and can be seen in Fig. 16.

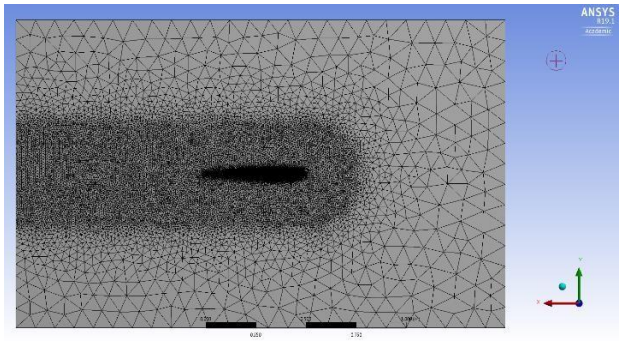

Figure 16. Mesh of domain and wing

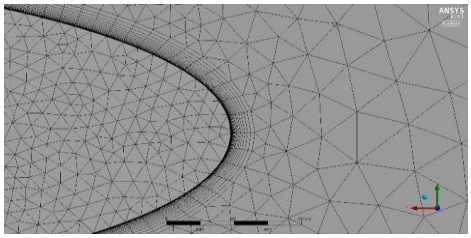

Figure 17. Boundary layers

The Shear Stress Transport (SST) model uses a combination of k-ε & k–ω depending on the location it is solving. Combining the best of the mentioned models helps in making a robust model that can tackle both near and far wall interaction with a good level of accuracy [17]. Thus, SST was the model used in this study.

The wind tunnel in this study had a symmetry plane with an arm balance. The symmetry plane was attached to the wing and the balance system was used to collect values for lift and drag. The uncertainty for each measurement was based on the limitations of the wind tunnel specification as seen in table (1). In addition, this setup was limited to 15° angle of attack due to the arm limitation of the wind tunnel setup.

Table 1. Taken from UWE Wind Tunnel Limitations

Component	**Range [N]**	**Uncertainty [N]**
Lift	±450	0.5
Drag	+80,-150	0.17(+),0.28(-)
Instrument	**Uncertainty**	**Unit**
Angle of Attack	0.3	Degrees

The formulas needed to calculate the upper and lower boundaries for the uncertainty can be found in Bell S. [16]

$$u(Cl) = |Cl_{Value}| \sqrt{\left(\frac{Lift_u}{Lift_{Value}}\right)^2 + \left(\frac{q_u}{q_{Value}}\right)^2 + \left(\frac{Length_u}{Length_{Value}}\right)^2 + \left(\frac{Width_u}{Width_{Value}}\right)^2}$$

$$u(Cd+) = |Cd_{Value}| \sqrt{\left(\frac{Drag+_u}{Drag_{Value}}\right)^2 + \left(\frac{q_u}{q_{Value}}\right)^2 + \left(\frac{Length_u}{Length_{Value}}\right)^2 + \left(\frac{Width_u}{Width_{Value}}\right)^2}$$

$$u(Cd-) = |Cd_{Value}| \sqrt{\left(\frac{Drag-_u}{Drag_{Value}}\right)^2 + \left(\frac{q_u}{q_{Value}}\right)^2 + \left(\frac{Length_u}{Length_{Value}}\right)^2 + \left(\frac{Width_u}{Width_{Value}}\right)^2}$$

Where u is the uncertainty for each point.

5. Experimental Wind Tunnel and CFD results

Wind tunnel results of Cd (with error boundaries) versus Angle of Attack (AoA) for morphing and hinged flap are shown in Fig. 18.

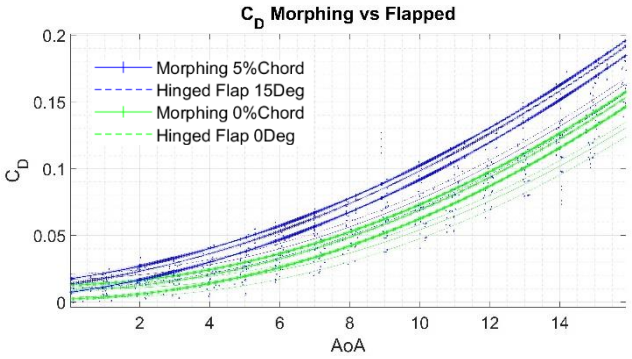

Figure 18. Cd vs AoA for both zero and 5% chord deflection.

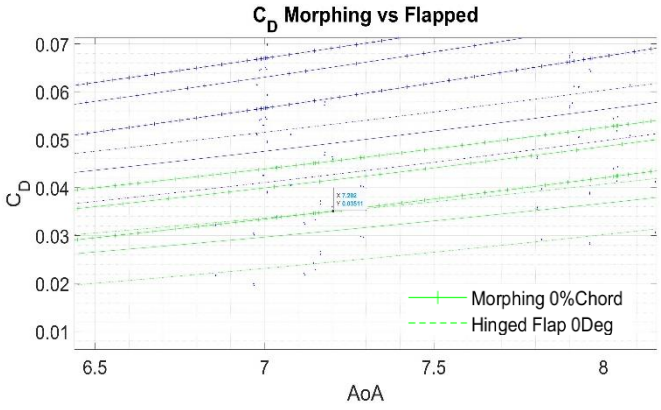

Figure 19. Cd vs AoA zoomed for zero flap deflection

Fig. 19 shows the point where Cd values error range for the morphing wing diverge from the hinged flap. This could indicate that for zero flap deflection the morphing wing Cd value could be greater than the hinged flap wing for angles above 7.2° ± 0.3 in this case.

Fig. 20 shows the point where Cd values error range for the morphing wing diverge from the hinged flap.

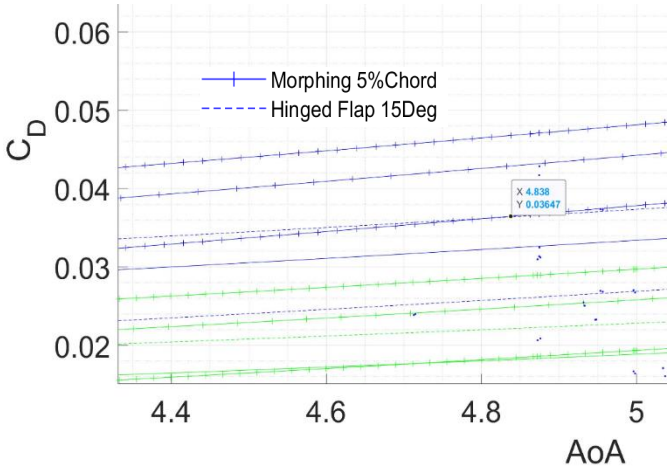

Figure 20. Cd vs AoA zoomed for 5% chord deflection (15°)

This might indicate that for 5% flap deflection the morphing wing Cd value could be greater than the hinged flap wing for angles above 4.8° ± 0.3.

Results for Cl values (with error boundaries) versus AoA for morphing and hinged flap are shown in Fig. 21 this may indicate that the morphing wing achieves a consistently higher Cl values for 5% chord deflection compared to its equivalent counterpart at 15° hinged flap.

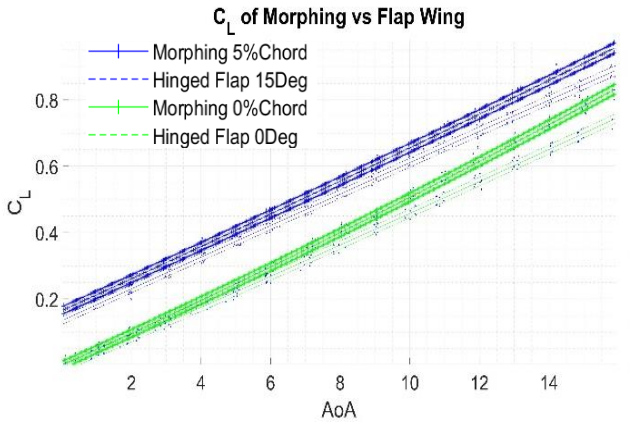

Figure 21. Cl vs AoA for both zero and 5% chord deflection

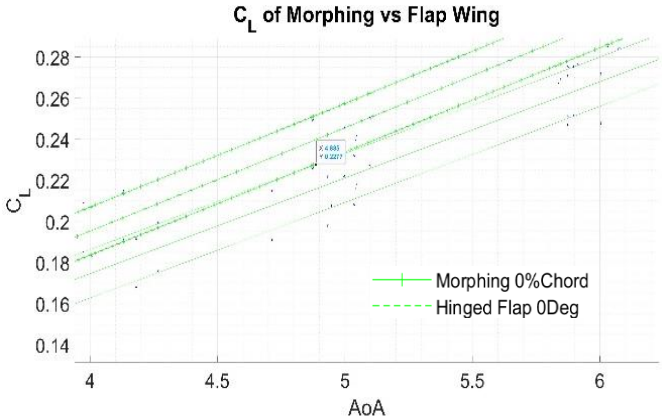

Figure 22. Cl vs AoA zoomed for zero flap deflection

From Fig. 22 morphing wing Cl values may be similar to hinged flap for angles up to 4.8° as seen in their error boundaries intersections.

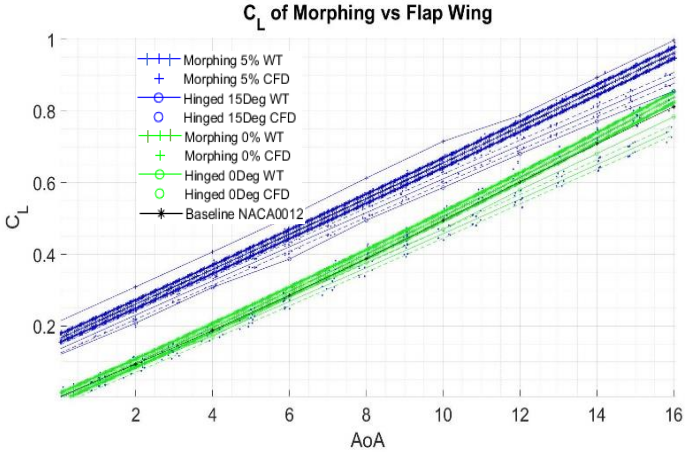

Figure 23. Cl vs AoA for both zero and 5% chord deflection Wind tunnel and CFD

Fig. 23 shows the Cl combination of wind tunnel and CFD results. The baseline NACA0012 Cl results lie in the uncertainty region of the morphing wing with no deflection. This is a respectable indication that experimental Cl results are consistent with the simulation results.

6. Conclusion

This study aimed to design, manufacture and test a morphing flapped wing and compare it to a single hinged flapped wing. The study's wind tunnel results show that using a morphing flapped wing rather than a conventional single hinged flapped wing could experience an average increase in lift

Cl values of 25.5% for morphing flap with no deflection. Cl increase of 15.4% for morphing flap deflection of 5% chord length (15°) and a 10.5% increase for of morphing flap at 10% chord length (30°) for this particular study are also observed. Although this study did not achieve the same additional lift increase, the trends seen for increasing lift are in line with studies carried out by [1] [6] [9].

Drag results from the wind tunnel of this study showed the region where the morphing wing with flap deflection of 5% chord length (15°) could have similar Cd results with its equivalent hinged flapped wing at between angles of attack of 0° and up to 4.8° ± 0.3. These results show a possible area where morphing and hinged flapped wing may provide similar properties for drag. Moreover, results for zero flap deflection showed similar drag values for both morphing and hinged wing from 0° up to angles of 7.2° ± 0.3. The range of angles seen in the results of this study lies in the region of trends seen by [1], despite the different setup. However, since uncertainties are significantly high in the regions of low angle of attack, it is difficult to state with complete confidence. Repeating the experiment might reduce uncertainty.

Cl results on the other hand showed a consistent increase in the lift coefficient values for the morphing wing compared to the hinged flap wing. The combinations of increased Cl values with similar or lower Cd values between certain angles of attack could lead to an improved aerodynamic performance between stated angles.

Fig. 24 presents vortex core regions for hinged flap and morphing wing. The morphing wing shows a more core uniform distribution along the flap section compared to the hinged wing. Similarly as seen in Fig. 25 results of [1] show the wing streamline vectors on flap to have common features as this study. However, there is a noticeable deference in tip vortex regions seen in this study since the setup did not use symmetry plain at the wing tip.

In summary, this study was able to show some of the different characteristics that could arise from a morphing and hinged flapped wing. This experiment has produced additional evidence that may support results seen in previous studies such as [1] [6] [9] despite the slightly different set up used. Moreover, this new design used in this study has shown the possibility of implementing and replacing hinged flaps with morphing flaps using a sliding mechanism improving performance as seen in results.

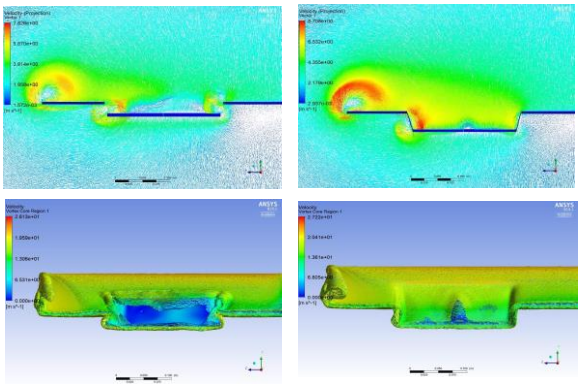

Figure 24. (Left) Hinged Flap Vortex Regions and (Right) Morphing Vortex Regions

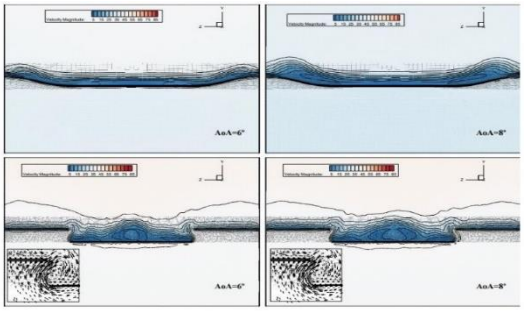

Figure 25. (Top) Morphing wing Streamlines and (Bottom) Hinged Flap wing. Taken from [1]

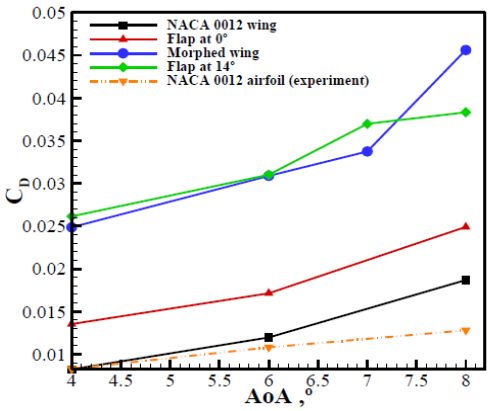

Figure 26. CFD Results for Cd from [1]

References

1. Abdessemed, C., Yao, Y., Bouferrouk, A. and Narayan, P. (2018) Analysis of a 3D Unsteady Morphing Wing with Seamless Side-edge Transition. *2018 Applied Aerodynamics Conference*, Atlanta, Georgia, 25-29 July 2018.Aviation Forum.

2. Piwek, K. and Wiśniowski, W. (2016) Small air transport aircraft entry requirements evoked by FlightPath 2050. Aircraft Engineering and Aerospace Technology 88(2), pp.341-347.

3. Macaraeg, M. (1998) Fundamental investigations of airframe noise. *4th AIAA/CEAS Aeroacoustics Conference.* Toulouse, France, 2-4 June 1998. AIAA Meeting Paper.

4. Macaraeg, M. (1998) Fundamental investigations of airframe noise. *4th AIAA/CEAS Aeroacoustics Conference* [online]. Toulouse, France, 2-4 June 1998. AIAA Meeting Paper.

5. Madi, F. (2018) *An investigation of morphing camber aerofoil*, Dissertation. Meng part A, University of the West of England

6. Dayyani, I., Khodaparast, H., Woods, B. and Friswell, M. (2014) The design of a coated composite corrugated skin for the camber morphing airfoil. *Journal of Intelligent Material Systems and Structures.* 26 (13), pp.1592-1608.

7. Dayyani, I., Khodaparast, H., Woods, B. and Friswell, M. (2014). The design of a coated composite corrugated skin for the camber morphing airfoil. *Journal of Intelligent Material Systems and Structures.* 26 (13), pp.1592-1608.

8. Concilio, A., Dimino, I., Lecce, L. and Pecora, R. (2018) *Morphing Wing Technologies. Large Commercial Aircraft and Civil Helicopters.*

9. Bolonkin A., Gilyard G. B. (1999) *Estimated benefits of variable-geometry wing camber control for transport aircraft.* NASA Center for Aerospace Information (CASI).

10. Ruangjirakit, K. (2013) *Polyurethane Corrugated Composites for Morphing Wing Applications* PhD. Imperial College London.

11. McGowan, Anna-Maria R. Vicroy, Dan D. Busan, Ronald C. Hahn, Andrew S. (2009) Perspectives on Highly Adaptive or Morphing Aircraft. *NATO RTO AVT-168 Symposium*. Lisbon, Portugal, 20-24 April 2009. Langley Research Centre.

12. Wickenheiser, A. and Garcia, E. (2007). Aerodynamic Modeling of Morphing Wings Using an Extended Lifting-Line Analysis. *Journal of Aircraft* 44(1), pp.10-16.

13. Jha, A. and Kudva, J. (2004) Morphing aircraft concepts, classifications, and challenges. *Industrial and Commercial Applications of Smart Structures Technologies,* Proceedings of SPIE Vol. 5388: 213 – 224

14. Anderson, John. (2017) *Fundamentals of Aerodynamics*. 6th Edition. New York: Mc Graw Hill Education.

15. Selig, M., Deters, R. and Wiliamson, G. (2011) Wind Tunnel Testing Airfoils at Low Reynolds Numbers. 49th AIAA Aerospace Sciences Meeting. Orlando, Florida, 4-7 January 2011.

16. Bell, S. (1999) A Beginner's Guide to Uncertainty of Measurement: National Physical Laboratory Issue 2. Teddington, Middlesex, United Kingdom.

17. Todorov, D. (2015) Aerodynamic Characteristics of Airfoil with Single Slotted Flat for Light Airplane Wing. International Conference of Scientific Paper AFASES 2015, Brasov, 28-30 May 2015.